Asian Journal of Pharmaceutical Sciences 17 (2022) 129–138

Available online at www.sciencedirect.com

ScienceDirect

journal homepage: www.elsevier.com/locate/AJPS

Original Research Paper

Amphiphilic small molecular mates match hydrophobic drugs to form nanoassemblies based on drug-mate strategy

Leiqiang Han[‡], *Shuang Liang*[‡], *Weiwei Mu, Zipeng Zhang, Limin Wang, Shumin Ouyang, Bufan Yao, Yongjun Liu*[*], *Na Zhang*[*]

Department of Pharmaceutics, Key Laboratory of Chemical Biology (Ministry of Education), School of Pharmaceutical Sciences, Cheeloo College of Medicine, Shandong University, Jinan 250012, China

ARTICLE INFO

Article history:
Received 11 March 2021
Revised 25 November 2021
Accepted 25 November 2021
Available online 30 November 2021

Keywords:
Drug-mate strategy
Molecular level
Hydrophobic drug
Small molecular mate
Nanoassemblies

ABSTRACT

Nanomedicine has made great progress in the targeted therapy of cancer. Here, we established a novel drug-mate strategy by studying the formulation of nanodrugs at the molecular level. In the drug-mate combination, the drug is a hydrophobic drug that is poorly soluble in water, and the mate is an amphiphilic small molecule (SMA) that has both hydrophilic and lipophilic properties. We proposed that the hydrophobic drug could co-assemble with a suitable SMA on a nanoscale without additive agents. The proof-of-concept methodology and results were presented to support our hypothesis. We selected five hydrophobic drugs and more than ten amphiphilic small molecules to construct a library. Through molecular dynamic simulation and quantum chemistry computation, we speculated that the formation of nanoassemblies was related to the binding energy of the drug-mate, and the drug-mate interaction must overcome drug-drug interaction. Furthermore, the obtained SF/VECOONa nanoassemblieswas selected as a model, which had an ultra-high drug loading content (46%), improved pharmacokinetics, increased bioavailability, and enhanced therapeutic efficacy. In summary, the drug-mate strategy is an essential resource to design exact SMA for many hydrophobic drugs and provides a reference for the design of a carrier-free drug delivery system.

[*] Corresponding authors.
E-mail addresses: liuyongjun@sdu.edu.cn (Y. Liu), zhangnancy9@sdu.edu.cn (N. Zhang).
[‡] These authors contributed equally to this work.
Peer review under responsibility of Shenyang Pharmaceutical University.

https://doi.org/10.1016/j.ajps.2021.11.002

1. Introduction

Nanomedicine has been extensively explored for delivering hydrophobic drugs, which have the advantages of increased solubility, prolonged duration of exposure, selective delivery to the tumor, and an improved therapeutic index [1,2]. These delivery methods are undoubtedly effective, and several of them have been approved for clinical application [3,4]. However, development of nanoformulations often requires complex schemes involving novel material synthesis, purification, and supramolecular self-assembly, which present a variety of challenges, including low loading, drug release, and higher barriers to clinical translation [5,6]. Finding a more efficient strategy is highly desirable.

Carrier-free nanodrugs were developed in recent years. Compared with traditional nanodrugs, carrier-free nanodrugs possess many advantages: (1) self-assembly into stable nanoparticles; (2) high drug loading; (3) avoidance of tedious steps for preparing additional carriers; and (4) no carrier-induced toxicity and immunogenicity [7]. According to the type of assembly mechanism, carrier-free nanodrugs are classified as prodrug self-delivery and pure drug self-delivery. Prodrug self-delivery is usually synthesized by conjugating active drugs with other molecules via suitable chemical linkers, which can form a stable nanocompound to achieve drug self-delivery [8]. Our group has been committed to developing a prodrug delivery strategy [9,10]. In our previous work, the platinum-based prodrug carboplatin–lauric acid was developed, which can self-assemble into a stable nanodrug, and it showed better antitumor activity than free drugs [10]. Zheng et al. synthesized a library of conjugates, which turn hydrophobic drugs into stable nanodrugs [4]. Pure drug self-delivery is composed entirely of pharmacologically active molecules, which can be constructed by one drug alone or more than one drug, such as an amphiphilic drug–drug conjugate and disulfide-bond-based pure drug self-delivery system. For example, in yan group, the hydrophilic anticancer drug irinotecan (Ir) and the hydrophobic anticancer drug chlorambucil (Cb) were conjugated via a hydrolyzable ester linkage [11]. The amphiphilic Ir–Cb conjugate self-assembled into nanoparticles and exhibited a longer blood retention half-life compared with free drugs, which facilitated the accumulation of drugs in tumor tissues and promoted their cellular uptake. By inserting a single disulfide bond into hydrophobic molecules, small-molecule drugs could form nanodrugs [12]. For example, docetaxel (DTX) was conjugated with d-α-tocopherol succinate (VE) via a disulfide bond, which could self-assemble into a stable nanodrug [13]. These drugs, with some chemical modification, could form stable nanodrugs and achieve drug self-delivery. However, the above carrier-free nanodrug did not consider the proportion of drugs and rationality of drug combinations.

Differing from previous studies of nanodrugs, we established a novel drug-mate strategy by studying the co-assembly behavior of compounds at the molecular level. For the drug-mate combination, the “drug” represents hydrophobic drugs that are poorly soluble in water. The “mate” represents an amphiphilic small molecule that possesses both hydrophilic and lipophilic properties. This kind of small amphiphilic molecule was named small molecular mate (SMA), a molecular chaperone that can mediate the assembly of polypeptides into correct proteins in the cell [14]. We proposed that the hydrophobic drug could co-assemble with a suitable SMA into a nanodrug without additive agents. A library including five hydrophobic drugs and more than ten SMAs was constructed to support our hypothesis. Through molecular dynamic (MD) simulation and quantum chemistry computation, we speculated that the formation of nanoassemblies was related to the intermolecular interactions and the binding energy of hydrophobic drugs and the mate.

In this study, the co-assembly mechanism and structure-activity relationship were studied via MD simulation and quantum chemistry computation to prove our hypothesis, that SMA can turn hydrophobic drugs into nanoassemblies. This hypothesis has been explored in more than ten SMA and tested with five chemotherapy drugs: sorafenib (SF), 10-hydroxy camptothecin (HCPT), docetaxel (DTX), ibrutinib (IBR), and lapatinib (LAP). Their structures, dynamic properties, and assembly mechanisms at the molecular level have been explored. Based on the above study of structure and assembly behavior, we found that the formation of nanoassemblies was related to the binding energy of hydrophobic drugs and mates. Furthermore, the interaction between SMA and the hydrophobic drug should be stronger than that between the molecules of the hydrophobic drug itself, in forming nanoassemblies that are highly dispersed in water. Then, the obtained SF/VECOONa nanoassemblies (SF NS) was selected as a model for nanoassemblies. We believe that this drug-mate strategy could provide a reference for the design of a carrier-free drug delivery system.

2. Materials and methods

2.1. *Materials*

SF was provided by Biochempartner Co., Ltd. (Shanghai, China). HCPT, DTX, IBR, LAP, glycyrrhizic acid (G), and aescinate sodium (A) were purchased from Melone Pharmaceutical (Dalian, China). All other reagents of analytical purity grade were obtained commercially. Transmission electron microscopy (TEM) (HT7700, Japan) was used to evaluate the morphology of nanoassemblies. Zetasizer Nano ZS90 was used to evaluate the particle size and zeta potential of nanoassemblies. The content of SF in different formulations was analyzed by reverse-phase HPLC (Agilent 1200). A fluorescence spectrometer (Hitachi F-7000) was used to measure the fluorescence. Near-infrared fluorescence (NIRF) imaging was obtained using a NIRF imaging system (IVIS Kinetic, USA). The fluorescence intensity of major organs and tumors was analyzed by Living Image software 3.1 (Caliper Life Sciences).

Human hepatocarcinoma cells (HepG2) were cultured in RPMI-1640 (with 10% fetal bovine serum) at 37°C with 5% CO_2. Mouse hepatocarcinoma cells (H22) were cultured in mice with ascites. Female Kunming mice were purchased from the Experimental Animal Center of Shandong University (Jinan, China). These experiments were performed according to the requirements of the Animal Management Rules of PRC (Approval No. 19030).

2.2. SMA screen and SAR study

To screen suitable SMA for hydrophobic drugs and obtain stable nanoassemblies, a library of small amphiphilic stabilizers was used to evaluate the co-assembly ability with hydrophobic drugs by the nanoprecipitation method. For example, SF and VECOOH (molar ratio = 1:1) were dissolved in dimethyl sulfoxide (DMSO), and 40 μl DMSO solution of SF and VECOOH at a fixed molar ratio was added into 960 μl deionized water with stirring. The mixed solution was dialyzed (MWCO = 3500) against ddH_2O to remove DMSO and obtain SF NS (SF: 1 mg/ml). Other nanoassemblies, including HCPT/G, SF/G, DTX/G, HCPT/A, SF/A, DTX/A, IBR/A, LAP/A, IBR/IBR, DTX/DTX, and LAP/LAP, were prepared by the same method as SF NS, and the final concentration of hydrophobic drugs was 0.5 mg/ml.

2.3. Characterization of SF NS

The size, polydispersity index (PDI), and zeta potential of nanoassemblies were determined by dynamic light scattering (DLS). The morphology of SF NS was observed by TEM. The amount of loaded SF was measured at wavelength 265 nm by using the HPLC method with a C_{18} chromatographic column. The mobile phase was acetonitrile and 0.03% aqueous triethylamine (63:37, v/v), the detection wavelength was 265 nm, and the flow rate was 1.0 ml/min. Drug loading efficiency (DL%) of SF in SF NS was quantified according to the following equation:

$$DL\% = \frac{\text{Amount of SF in SF NS}}{\text{Amount of SF NS}} \times 100$$

2.4. Stability evaluation

The dilution stability, storage stability, and plasma stability of obtained SF NS were evaluated. Dilution stability: SF NS was diluted with water (2, 4, 8, 16, 32, 64, 128, 256 and 512 times), then the particle size and PDI of SF NS were measured by DLS. Storage stability: SF NS was stored for 120 h at room temperature, then the particle size and PDI of SF NS were measured by DLS. Plasma stability: SF NS were mixed with 20% mice plasma for 24 h, then the particle size and PDI of SF NS were measured by DLS.

2.5. Ultraviolet visible (UV) absorption

UV absorption of SF, VECOONa, SF NS and SF/VECOONa mixture with a concentration of 1 mg/ml SF or VECOONa in water or methanol were determined. In addition, the UV spectrum of SF, VECOONa, and SF/VECOONa mixture with equal concentration of SF in H_2O/CH_3OH (3/1, v/v) was measured with a UV-VIS spectrophotometer (TU-1810, Beijing Puxi General Instrument Co., Ltd.).

2.6. X-ray diffraction analysis

The crystalline nature of lyophilized SF NS was analyzed with an X-ray diffractometer (Advanced D8 X-ray Diffraction Analyzer, Karlsruhe, Germany). Samples of lyophilized SF NS without cryoprotectant, SF powder, and VECOOH powder were measured.

2.7. In vitro release of SF

In vitro release of SF was carried out by adding 1 ml of different formulations into a dialysis bag. Then, the dialysis bag was immersed into 10 ml of pH 7.4 phosphate-buffered saline (PBS) containing 1% (w/v) Tween 80 and kept at 37 °C in a shaker at 100 rpm. At predetermined time points (0.5 h, 1 h, 2 h, 4 h, 6 h, 8 h, 12 h, 24 h and 48 h), the release medium was withdrawn followed by addition of 10 ml of fresh PBS. The amount of SF released from different formulations in the release medium was measured by HPLC as described above. The release experiment was performed in triplicate.

2.8. Quantum chemistry computation

Computation principle: The molecular dynamics method and quantum chemistry method can be employed to calculate both the coarse and accurate binding conformation. The conformation of the individual hydrophilic drug agent and the hydrophobic drug agent could be calculated by the quantum chemistry method to obtain the accurate individual conformation. The accurate binding conformation and individual conformation could be further adopted to calculate the free energy by the quantum chemistry method. Based on the free energy, the interaction between the hydrophilic drug molecule and hydrophobic drug molecule is equal to the free energy between the hydrophilic drug molecule and the hydrophobic drug molecule minus the free energy of individual hydrophilic drug molecule and the hydrophobic drug molecule; the interaction between the hydrophobic drug molecules themselves is equal to the free energy between the hydrophobic drug molecule itself minus the free energy of individual hydrophobic drug: Interaction Energy(A / B) = Free Energy (A / B)-Free Energy (A) – Free Energy (B)

Computation Method:

1. Molecular Dynamic Simulation: 22 drug-drug complex simulation models (DOX+/HCPT, IR+/SN-38, Ce63-/HCPT, ICG-/EPI, DOX+/UA, Ce62-/DOX, HCPT/HCPT, SN-38/SN-38, EPI/EPI, UA/UA, DOX/DOX, SF/SF, 1/SF, 2/SF, 3/SF, 4/SF, 5/SF, 6/SF, 7/SF, 8/SF, 9/SF, and 10/SF) were built in the MOE (molecular operating environment) software package. The initial position of the drug molecules in each simulation mode was random. The prepared model was solvated in a box and neutralized using the Amber tool package [15]. Before the MD simulation, the force field parameters were added onto the drug molecules and water box. The TIP3P model and Amber99SB force field were employed for the water molecules, and the force field [16–18] parameters of drug molecules were generated from the general Amber force field (GAFF) [19]. The force field parameters lacking in GAFF were supplemented by using the antechamber [20] procedure in Amber14. The MD simulations were preceded by using the pmemd procedure of the GPU-accelerated Amber14 package. First, the solvent was relaxed while the drug molecules were constrained;

Second, the heavy atoms of the drug molecules were constrained while relaxed the hydrogen atoms of the drug molecules and the water molecules were relaxed; Third, all the molecules were minimized without any restrictions. After three-step minimization, each model was gradually heated from 0 to 300 K over a period of 50 ps. Afterward, approximately 50 ns of NVT MD simulation were performed for each model. Meanwhile, the Berendsen method [21], Beeman algorithm [22], as well as the SHAKE algorithm [23] were used to regulate system temperature, analyze the Newtonian equation of motion, and constrain the hydrogen-containing bonds, respectively. The 50 ns MD simulations could calculate the coarse binding conformation between the drug molecules in each model.

2. Quantum Chemistry Computation: The Gaussian 09 package was used to process the higher accuracy computation to obtain the more accurate binding conformation after the coarse binding conformation was obtained from the MD simulation. Firstly, the coarse binding conformation from the MD simulation was optimized and the simple harmonic frequency calculation processed at the B3LYP/6-31G* level to obtain the binding conformation of the local minimum point. Second, the binding conformation of the local minimum point was further processed by the single point energy and simple harmonic frequency calculation at the B3LYP/6-311+G* level [24] in the polarimetric continuous medium (PCM) [25] solvent model. From the simple harmonic frequency calculation, the free energy of the binding conformation of each model could be obtained. Meanwhile, at the same optimization level (B3LYP/6-31G*) and frequency calculation level (B3LYP/6-311+G*), each individual drug molecule was processed by conformation optimization and frequency calculation to obtain the free energy of individual drug molecules. Based on the free energy of binding conformations and individual drug molecule conformations (hydrophilic molecules and hydrophobic molecules), the interaction between the drug molecules could be calculated.

The initial structures of SF/8 and SF/9 systems were then constructed by the insert-molecules module. SF, compound 8, and compound 9 molecules were placed in a $6 \times 6 \times 6$ nm water box. The two systems were formed by 50 000 atoms. To run the MD simulations, the Gromacs 2018.4 package was used with the Charmm36 force field. Long-range electrostatics were calculated. For van der Waals interactions, a cutoff value of 1.0 nm was used. All hydrogen-related bonds were constrained by the LINCS algorithm. The V-rescale method was used to control the system temperature at 300 K, and the Parrinello–Rahman method was used to control the pressure at 1 bar. The SF/8 and SF/9 configurations were energy minimized and subjected to 100 ps NVT equilibration at 300 K. Then, the two systems were run for 50 ns of NPT production. The time step of simulation was 2 fs. The trajectories were saved every 10 ps, yielding a total of 5000 snapshots for production analysis.

2.9. Quantification of drug molecular interactions

Conformation search of drugs and different water-soluble molecules: Eleven different compound structures with molecular number ratios of 1:1 were constructed by Molclus. Twenty conformations were collected from each system, and MOPAC [26] was used for preliminary optimization of each conformation and extraction of the lowest energy conformation. Optimization of complex structure and calculation of interaction energy: The complex structure obtained by Molclus was optimized at the level of B3LYP/6-31g* [27], and the binding energy was calculated at the level of the 6-311+G* base group [28]. The Basis Set Superposition Error (BSSE) was added in the calculation [29,30]. The final binding energy was calculated by the following formula:

$$E_{interaction} = E_{complex} - E_{template} - E_{monomer} + E_{BSSE},$$

where $E_{complex}$ is the energy of the complex, $E_{template}$ is the energy of the template molecule, $E_{monomer}$ is the energy of the monomer molecule, and E_{BSSE} is the corrective energy of BSSE.

It has been reported that urea and detergent sodium dodecyl sulfate (SDS) can destroy hydrogen bonds and hydrophobic interaction [31,32]. Therefore, we further selected urea and SDS to destroy hydrogen bonds and hydrophobic interaction at final levels of 5 mmol/l and 4 mol/l, respectively. The size and morphology were studied via DLS and TEM.

2.10. In vitro cytotoxicity

In vitro cytotoxicity of VECOOH, SF solution, and SF NS were evaluated in HepG2. Briefly, HepG2 cells were seeded in a 96-well plates (5000/well). After 12 h, these cells were treated with VECOOH, SF solution, and SF NS at different concentrations. After 48 h, 20 μl of MTT (5 mg/ml) was added. Then after 4 h, 150 μl DMSO was added. The absorbance value was read at 570 nm. Cell viability was calculated according to the following equation:

$$\text{Cell viability (\%)} = \frac{Abs_{sample} - Abs_{sample}}{Abs_{control} - Abs_{blank}} \times 100\%$$

2.11. Pharmacokinetic study

For pharmacokinetic studies, female Kunming mice (~20 g) were randomly divided into three groups including SF solution (iv), SF NS (iv) and SF suspension (po) at a dose of 10 mg/kg. The blood samples were obtained from the retro-orbital plexus at preset times. Then, 400 μl plasma was obtained from whole blood and mixed with 800 μl protein precipitation solution (acetonitrile: methanol = 2:1, v/v) followed by vortexing for 1 min to precipitate plasma proteins and then centrifugation. Then the supernatant was filtered and analyzed by HPLC. The main pharmacokinetic parameters were analyzed using DAS 2.0 software.

2.12. In vivo antitumor efficacy

The *in vivo* antitumor activity of SF NS was determined by a line of mice bearing H22 cells. When the tumor reached

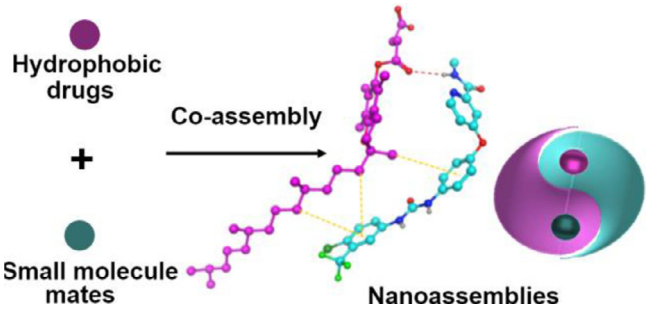

Scheme 1 – Tailor-made small molecular mates co-assembled with the hydrophobic drugs to form stable nanoassemblies based on the drug-mate strategy.

a certain volume (~100 mm^3), these mice were randomly divided into three groups: control (normal saline), SF solution (10 mg/kg), and SF NS (10 mg/kg). Various formulations were injected on days 1, 4, 7, 10, 13, 16 and 19. Tumor length and width and body weight were measured on days 1, 7, 13, 19 and 25. The volume of tumor was calculated according to the following formula:

$$\text{Tumor volume}\left(mm^3\right) = 0.5 \times \text{length} \times \text{width}^2$$

Then these mice were euthanized, and the excised tumors in the different groups were weighed and evaluated via Tunel staining.

2.13. *In vivo safety*

The *in vivo* safety of SF NS on main organs was evaluated. The main organs of the mice in the "*in vivo* antitumor efficacy" group were dissected and stained with H&E for histopathological examination. Blood samples of the mice in the *in vivo* antitumor efficacy group were obtained. White blood cells (WBC), red blood cells (RBC), hemoglobin (HGB), and platelets (PLT) in whole blood were measured to evaluate myelosuppression. The levels of glutamic transaminase (ALT), aspartate transaminase (AST), creatinine (CRE), and blood urea nitrogen (BUN) in the serum samples were analyzed to assess the toxicity in liver and kidney.

2.14. *Statistical Analysis*

Statistical differences between t groups were evaluated by the *t*-test, one-way or two-way ANOVA. When $P < 0.05$, differences were considered to be statistically significant.

3. Results and discussion

3.1. *Preliminary co-assembly behavior evaluation of SF with SMA*

We initially built a library to verify our hypothesis that a hydrophobic drug could co-assemble with suitable SMA into nanodrugs without additive agents. SF was chosen as a model drug because its clinical application has been significantly restricted by its water-insoluble property. More importantly, it is difficult to chemically modify SF, and most nanoformulations of SF have been prepared through physical encapsulation using large quantities of pharmaceutical excipients [33–39]. Ten biocompatible small molecules (Fig. 1**A**) were designed as candidate SMAs. Through screening, when 8 (D-α-Tocopherol succinate, VECOONa) (Fig. 1**A**) and SF in equal molar ratios were dissolved in DMSO together and then water was added, a stable colloidal solution was formed (Fig. 1**B**) without any precipitation even after removing DMSO by dialysis (SF, 1 mg/ml). The resulting SF nanoassemblies (SF NS) exhibited spherical morphology (Fig. 1**B**).

To understand how the molecules interact with each other in aqueous solution, MD simulations were carried out. 8 and 9 possessed the same hydrophobic moiety and various hydrophilic groups were chosen, and their MD simulation for 8/SF and 9/SF were extracted. After 50 ns, 8 co-assembled with SF into nanoassemblies, showing a large number of hydrophilic groups (red) of 8 on the surface (Fig. 1**C**). 9 with SF did not completely form into complex. The hydrogen bond is a common strong force in the assembly of nanoassemblies. In order to study the driving forces of assembly of 8/SF and 9/SF, the number of hydrogen bonds between nanoassemblies and solvent and within nanoassemblies during MD simulation was analyzed. As shown in Fig. 1**D**-1**E**, the number of hydrogen bonds between 9/SF and water molecules was approximately 50% of 8/SF. The hydrogen bond number within 8/SF was obviously more than that of 9/SF, indicating that the binding force between SF and 9 was relatively weak. Moreover, the density (Fig. 1**F**) of 8/SF (>300 kg/m^3) in the center of the box was significantly higher than that of 9/SF (<150 kg/m^3), which indicated 9/SF was more dispersed in the assembly process. With the assembly of nanoassemblies, the area exposed to the solvent environment will gradually decrease, so the solvent- accessible surface area (SASA) can be used to evaluate the compactness of nanoassemblies. It can be seen from Fig. 1**G** that SASA values of both systems decreased significantly during the MD process. Specifically, the SASA value of the 8/SF system decreased more than that of 9/SF, indicating that the former formed more compact nanoassemblies. All these results were consistent with our experimental data and strongly supported the hypothesis that SF and 8 molecules co-assembled into stable nanoassemblies.

In addition to hydrogen bonding, hydrophobic interaction also plays an important role in nanoassemblies. To study the co-assembly behavior more accurately, quantum chemistry computation was used to calculate the molecular interaction forces. The computation results are listed in Fig. 1**H**. Some molecules could form stronger interactions with SF, i.e., 8/SF > 5/SF > 2/SF > SF/SF ≈ 6/SF, and the binding energy of 8/SF was below -20 Kcal/mol; however, some formed weaker interactions with SF. Structurally (**Fig. S1**), molecules 2, 5, and 6 had more 1~3 double bonds than molecules 1 and 7. Because of the double bond, molecules 2, 5, and 6 could fold and wrap the hydrophobic drug molecule SF to form more CH-π stacking from multiple directions. Some studies [40–45] have reported that an amphiphilic anticancer agent could co-assemble with a hydrophobic anticancer agent. Their

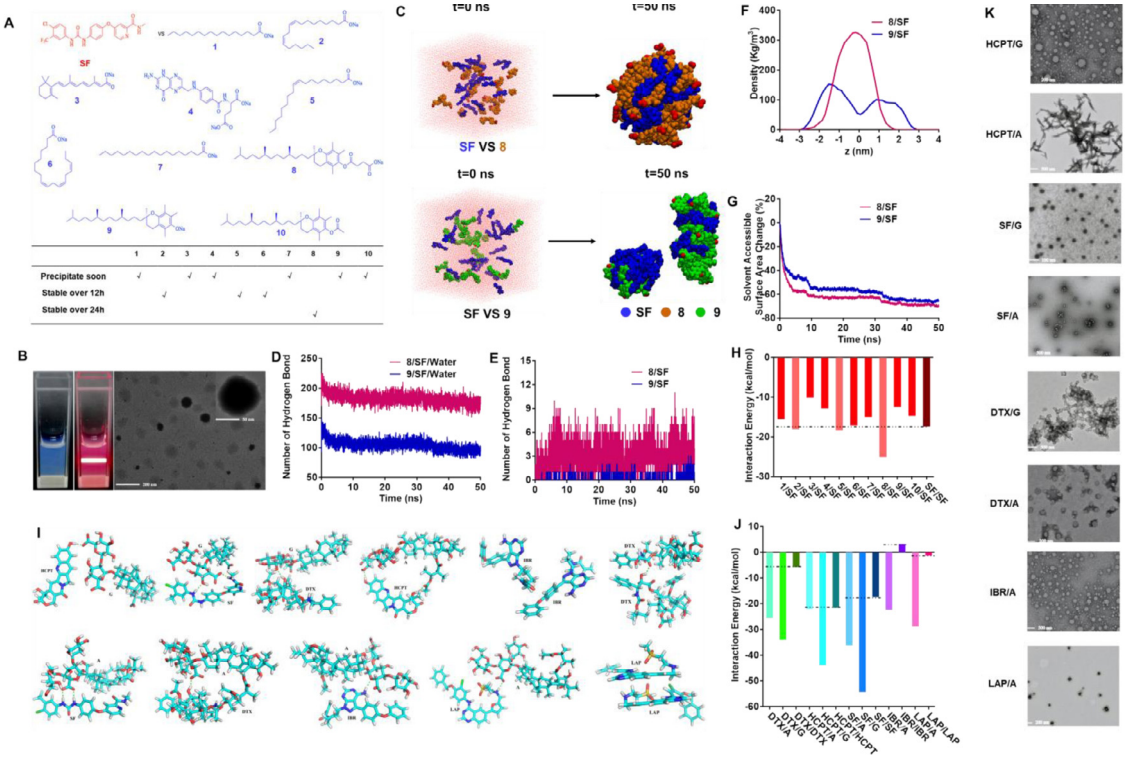

Fig. 1 – Preliminary co-assembly behavior evaluation of SF with SMA. (A) The library of SMA used for evaluation to co-assemble with SF. (B) Appearance and TEM image of SF NS. (C) MD simulations of the co-assembly of 8/SF and 9/SF molecules in water after 50 ns, respectively. (D) The number of hydrogen bonds in the co-assembly process between nanoparticles with water. (E) The number of hydrogen bonds between SF with 8 or 9. (F) Density distribution of the co-assembly system. (G) Variation of solvent-accessible surface area of the co-assembly system with time. (H) Interactions between hydrophobic and amphiphilic molecules: SF with different amphiphilic molecules. (I) The co-assembly conformations of HCPT/G, SF/G, DTX/G, HCPT/A, SF/A, DTX/A, IBR/A, LAP/A, IBR/IBR, DTX/DTX, and LAP/LAP. (J) Calculation of intermolecular interaction forces. (K) TEM images of the formed nanoassemblies.

interaction forces were also calculated and are shown in **Fig. S1-S2**, i.e., DOX^+/HCPT > HCPT/HCPT, IR^+/SN-38 > SN-38/SN-38, $Ce6^{3-}$/HCPT > HCPT/HCPT, ICG^-/EPI > EPI/EPI, DOX^+/UA > UA/UA, and $Ce6^{2-}$/DOX > DOX/DOX. Their experimental results were in agreement with our calculated results. These results demonstrated that when binding energy is below -20 Kcal/mol, an amphiphilic SMA with an equal molar ratio can co-assemble with a hydrophobic drug via strong interaction, overcome the interaction of the hydrophobic drug with itself, and eventually form nanoassemblies that are highly dispersed in water. We named the phenomenon the drug-mate strategy. This finding using SMA to turn hydrophobic drugs into nanoassemblies showed great potential for drug delivery, which encouraged us to further verify the drug-mate strategy and explore more useful SMAs. We further constructed a library, in which two natural drugs glycyrrhizic acid (G) and aescinate sodium (A) were chosen to carry hydrophobic drugs, such as SF, HCPT, DTX, IBR, and LAP. Almost all of them showed hydrogen bonds with drug molecules (Fig. 1I) and binding energy was below -20 Kcal/mol (Fig. 1J). SF/G, SF/A, HCPT/G, HCPT/A, DTX/A, DTX/G, IBR/A, and LAP/A all co-assembled into nanostructures (Fig. 1K). These results supported the drug-mate strategy, that SMA could transform hydrophobic drugs into nanoassemblies efficiently, with high drug loading.

3.2 . *Characterization of SF NS*

The obtained SF NS was selected as model to evaluate its physicochemical properties. The resulting SF NS exhibited uniform size (91.55 ± 1.87 nm, PDI 0.102 ± 0.007), and zeta potential of -33 mV in water (Fig. 2A). More importantly, it had an ultra-high drug load of 46%, compared with the lipid-based SF nano suspensions (11%) and SF liposomes (4%) prepared by our group. The formation of SF NS should be ascribed to the strong interaction force between SF and VECOONa. The ultraviolet-visible (UV) absorption of SF, VECOONa, SF NS, and the SF/VECOONa mixture was shown in Fig. 2B. SF and the SF/VECOONa mixture in CH_3OH had the same maximum absorption at 265 nm, while VECOONa had very little absorption. When SF and VECOONa co-assembled together, the maximum absorption wavelength red-shifted to 269 nm. In addition, the UV spectrums of SF, VECOONa, and SF/VECOONa mixture (in H_2O/CH_3OH=3/1, v/v) are shown in Fig. 2C, indicating that the solvent water in SF NS made no contribution to the red shift. This verified our conclusion that SF NS was formed from the interaction between heterogeneous molecules.

The strong interaction force between SF and VECOONa also contributed to the stability of SF NS. As shown in

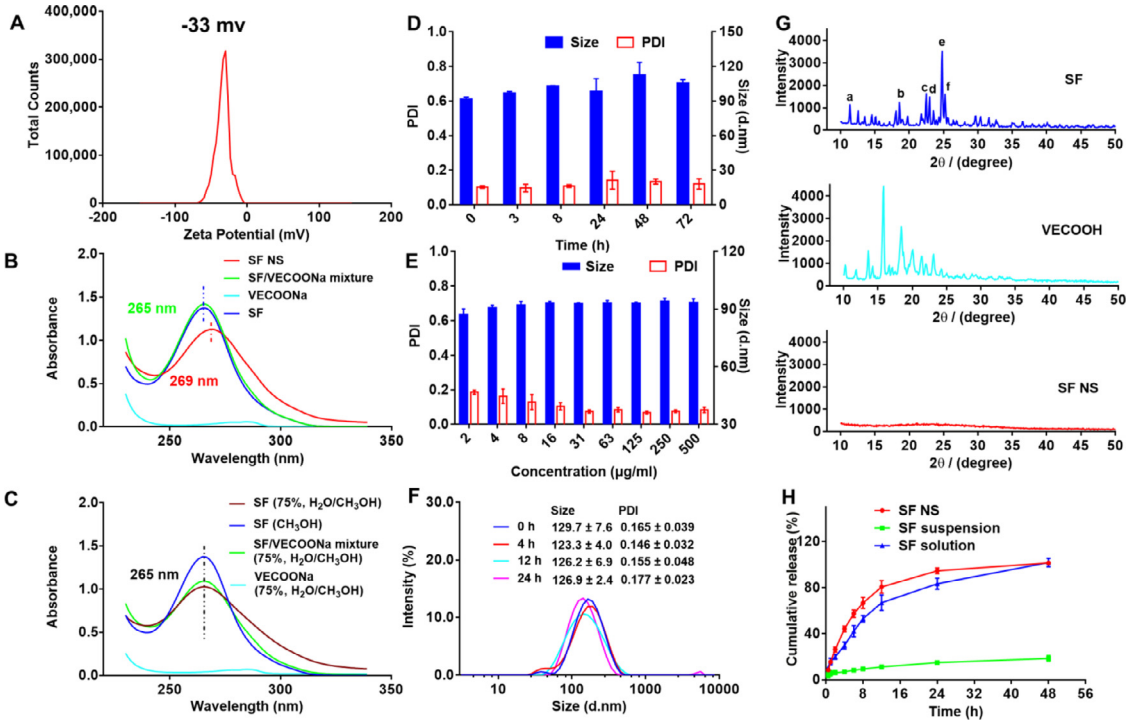

Fig. 2 – The obtained SF NS was selected as a model to evaluate its physicochemical properties. (A) Zeta potential of SF NS. (B) The UV spectrum of SF, VECOONa, SF NS, and the SF/VECOONa mixture. (C) The UV spectrum of SF, VECOONa, and the SF/VECOONa mixture in H_2O/CH_3OH (3/1, v/v). (D) Stability of SF NS after storage for 72 h at room temperature (n = 3). (E) Changes in particle sizes and PDI of SF NS diluted in water (n = 3). (F) Size distribution of SF NS with 20% plasma for 24 h at 37°C. (G) X-RD diagrams of SF NS, SF, and VECOOH. (H) *In vitro* release profile of SF from SF NS, SF suspension, and SF solution in PBS (pH =7.4).

Fig. 2D, SF NS remained well dispersed at 72 h at room temperature. When it was diluted into 2 μg/mL, the particle size remained almost unchanged (Fig. 2E). Because the SF NS is intended to be administered intravenously, its stability in 20% mouse plasma was further evaluated. As shown in Fig. 2F, the size of SF NS remained stable for 24 h, suggesting tolerance of SF NS in the bloodstream. In addition, as shown in Fig. 2G, the strong Bragg peaks in the diffraction patterns of SF (a, 11.36°; b, 18.56°; c, 22.48°; d, 22.96°; e, 24.80°; f, 25.20°) indicated its strong crystallization. In contrast, for the SF NS, these typical peaks disappeared, which implied that SF molecules randomly mixed with VECOONa molecules and were distributed in an amorphous state. According to the *in vitro* release profile of SF (Fig. 2H), the rapid release behavior of SF NS was observed, which is similar to that of SF solution (Cremophor EL:ethanol=1:1, v/v), while approximately 100% SF was released from SF NS, compared to about 20% from SF suspension.

These findings further verified our conclusion, that such an amorphous state might be advantageous in improving the dissolution rate and bioavailability of SF. In addition, we added a specific interaction inhibitory agent to demonstrate the existence of hydrogen bonds and hydrophobic interaction. The uniform size of SF NS disappeared with addition of a specific interaction inhibitory agent (urea or SDS). Moreover, the results of TEM showed the disassembly of SF NS with addition of urea or SDS (**Fig. S3**). These results further confirmed the existence of hydrogen bonds and hydrophobic interaction between hydrophobic drugs and SMA.

3.3 . *In vitro and in vivo antitumor activity of SF NS*

The proliferation inhibition (Fig. 3A) of SF NS was evaluated in a HepG2 cell line. The IC_{50} of SF NS was 3.44 ± 0.15 μg/ml, which was close to that of free SF (4.44 ± 0.24 μg/ml). The pharmacokinetics of SF NS, SF solution (iv) and SF suspension (po) are listed at a dose of 10 mg/kg in Fig. 3B and summarized in **Table S1**. SF is almost insoluble in water, and the oral bioavailability of SF suspension is extremely low. The plasma concentrations of SF in SF NS (iv) were higher than that of SF solution (iv) and SF suspension. The resulting AUC value of SF NS (90.1 μg•h/ml) was 2 times than that of SF solution (41.0 μg•h/ml), and was 20 times that of SF suspension (4.4 μg•h/ml). The improved bioavailability of SF NS is mainly due to increased solubility and dissolution. The *in vivo* anti-tumor activity (Fig. 3C) of SF NS was evaluated. Seven treatments of mice with SF solution at a dose of 10 mg/kg (eq. SF) every 3 d led to the highest inhibition of tumor growth compared with control ($P<0.01$). SF solution at the same dose showed only a modest inhibition efficacy. The tumor weight (Fig. 3D, Fig. 3E) in mice after treatment with SF NS was significantly lower than after SF solution ($P < 0.05$). Moreover, the validity of SF NS was assessed by TUNEL (Fig. 3F) staining of these tumors.

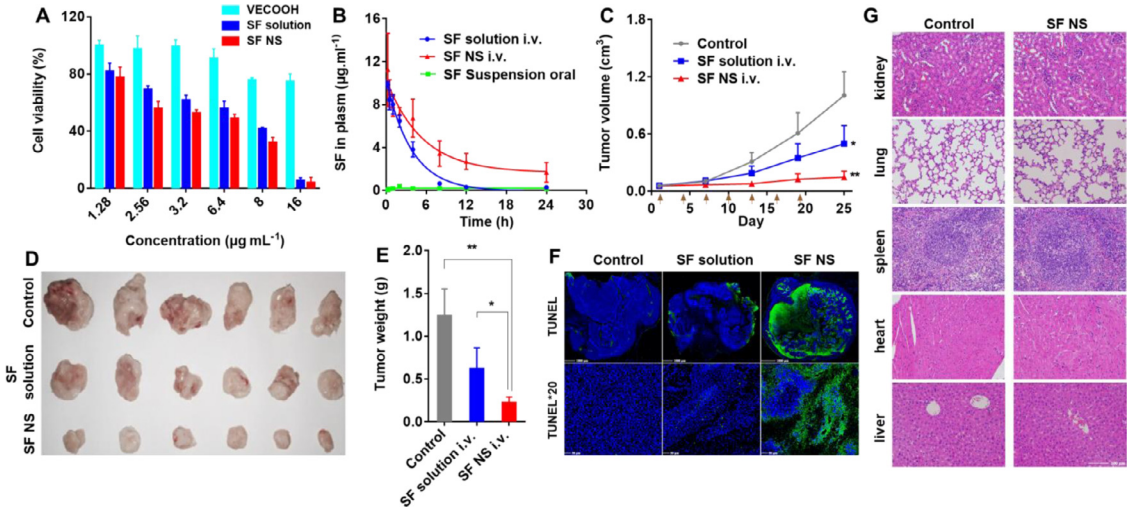

Fig. 3 – The model nanoassemblies SF NS showed good antitumor efficacy (A) *In vitro* cytotoxicity of VECOOH, SF solution, and SF NS in HepG2 cells at 48 h ($n = 3$). (B) The curves of SF concentration in plasma vs. time after SF NS (iv), SF solution (iv), or SF suspension (po) were administrated to mice (SF, 10 mg/kg, $n = 3$). *In vivo* antitumor efficacy study (C) tumor volume ($P < 0.01$, SF NS vs. control, SF solution; *$P < 0.05$, SF solution vs. control). (D) Photo of isolated tumors. (E) Average tumor mass isolated from the mice of each experimental group. Data are mean ± SD (n = 6) **$P < 0.01$, *$P < 0.05$. (F) Representative photographs of TUNEL-stained H22 tumor sections (below) and whole tumor slice scan (above). Positive apoptosis cells are green and nuclei stained with DAPI are blue. (G) H&E staining showing histopathological changes in major visceral organs.**

Tumors from the SF NS treated group exhibited more advanced cell apoptosis compared with the groups treated with physiological saline and SF solution. H&E (**Fig. S4**) staining of these tumors also showed the same results. The organs of the mice were harvested, sliced, and stained with H&E (Fig. 3G) to monitor the systemic toxicity of SF NS, which was compatible with the body weight changes in the mice (**Fig. S5**). A peripheral blood hemogram and liver and kidney toxicity were further evaluated to assess *in vivo* biosafety. The amount of WB, RBC, HGB and PLT showed no significant change in SF NS group compared with NS group ($P > 0.05$), which demonstrated the *in vivo* safety of SF NS with respect to the peripheral blood hemogram (**Table S2**). The level of liver enzymes and renal lesion indicators is shown in **Table S3**. The concentrations of ALT, AST, BUN and CRE in SF NS group showed no significant changes compared with in NS group. These results suggested that SF NS may be safe for liver and kidney *in vivo*.

4. Conclusion

In summary, we established a novel nanoassembly system at the molecular level, called drug-mate strategy. The co-assembly mechanism and structure-activity relationship were studied via MD simulation and quantum chemistry computation to prove our hypothesis that amphiphilic small molecules can turn hydrophobic drugs into nanoassemblies. We found that when binding energy was below -20 Kcal/mol, an amphiphilic small molecule with equal molar ratio can co-assemble with a hydrophobic drug via strong interaction, overcoming the interaction of the hydrophobic drug itself, and eventually form nanoassemblies that are highly dispersed in water. We presented a proof-of-concept methodology and results to support our hypothesis. This hypothesis has been explored through three SMAs and tested with five chemotherapy drugs. The obtained SF NS was selected as a model, which had an ultra-high drug loading content, improved pharmacokinetics, increased bioavailability, and enhanced therapeutic efficacy. Overall, the drug-mate strategy can be an essential resource to design exact SMA for some hydrophobic drugs and provide a reference for the design of a carrier-free drug delivery system. (Scheme 1)

Conflicts of interest

The authors declare no competing financial interests.

Acknowledgments

This work was supported by the National Natural Science Foundation of China (grant numbers: 81974498) and Natural Science Foundation of Shandong Province (grant numbers: ZR2019BH079). We thank the pharmaceutical biology sharing platform of Shandong University for supporting the cell platform in this work. We thank Translational Medicine Core Facility of Shandong University for the assistance with consultation and instrumentation in this work. We thank the Microscopy Characterization Facility of Shandong University for assistance with confocal laser scanning microscopy.

Supplementary materials

Supplementary material associated with this article can be found, in the online version, at doi:10.1016/j.ajps.2021.11.002.

REFERENCES

[1] Shi J, Kantoff PW, Wooster R, Farokhzad OC. Cancer nanomedicine: progress, challenges and opportunities. Nat Rev Cancer 2017;17:20–37.
[2] van der Meel R, Sulheim E, Shi Y, Kiessling F, Mulder WJM, Lammers T. Smart cancer nanomedicine. Nature nanotechnology 2019;14:1007–17.
[3] Ren G, Jiang M, Xue P, Wang J, Wang Y, Chen B, et al. A unique highly hydrophobic anticancer prodrug self-assembled nanomedicine for cancer therapy. Nanomedicine 2016;12:2273–82.
[4] Wang HX, Xie HY, Wang JG, Wu JP, Ma XJ, Li LL, et al. Self-assembling prodrugs by precise programming of molecular structures that contribute distinct stability, pharmacokinetics, and antitumor efficacy. Adv Funct Mater 2015;25:4956–65.
[5] Karaosmanoglu S, Zhou MJ, Shi BY, Zhang XJ, Williams GR, Chen XF. Carrier-free nanodrugs for safe and effective cancer treatment. J Control Release 2021;329:805–32.
[6] Ma W, Cheetham AG, Cui H. Building nanostructures with drugs. Nano today 2016;11:13–30.
[7] Qin SY, Zhang AQ, Cheng SX, Rong L, Zhang XZ. Drug self-delivery systems for cancer therapy. Biomaterials 2017;112:234–47.
[8] Wang Y, Cheetham AG, Angacian G, Su H, Xie LS, Cui HG. Peptide-drug conjugates as effective prodrug strategies for targeted delivery. Adv Drug Deliver Rev 2017;110:112–26.
[9] Han LQ, Wang TQ, Wu JL, Yin XL, Fang H, Zhang N. A facile route to form self-carried redox-responsive vorinostat nanodrug for effective solid tumor therapy. Int J Nanomed 2016;11:6003–22.
[10] Liang S, Han LQ, Mu WW, Jiang DD, Hou T, Yin XL, et al. Carboplatin-loaded SMNDs to reduce GSH-mediated platinum resistance for prostate cancer therapy. J Mater Chem B 2018;6:7004–14.
[11] Huang P, Wang DL, Su Y, Huang W, Zhou YF, Cui DX, et al. Combination of small molecule prodrug and nanodrug delivery: amphiphilic drug-drug conjugate for cancer therapy. J Am Chem Soc 2014;136:11748–56.
[12] Wang YJ, Liu D, Zheng QC, Zhao Q, Zhang HJ, Ma Y, et al. Disulfide bond bridge insertion turns hydrophobic anticancer prodrugs into self-assembled nanomedicines. Nano letters 2014;14:5577–83.
[13] Ren GL, Jiang MJ, Xue P, Wang J, Wang YJ, Chen B, et al. A unique highly hydrophobic anticancer prodrug self-assembled nanomedicine for cancer therapy. Nanomed-Nanotechnol 2016;12:2273–82.
[14] Hartl FU, Bracher A, Hayer-Hartl M. Molecular chaperones in protein folding and proteostasis. Nature 2011;475:324–32.
[15] Jorgensen WL, Chandrasekhar J, Madura JD, Impey RW, Klein ML. Comparison of simple potential functions for simulating liquid water. J Chem Phys 1983;79:926–35.
[16] Cornell WD, Cieplak P, Bayly CI, Gould IR, Merz KM, Ferguson DM, et al. A second generation force field for the simulation of proteins, nucleic acids, and organic molecules. J Am Chem Soc 1995;117:5179–97.
[17] Hornak V, Abel R, Okur A, Strockbine B, Roitberg A, Simmerling C. Comparison of multiple amber force fields and development of improved protein backbone parameters. Proteins 2006;65:712–25.
[18] Svozil D, Sponer JE, Marchan I, Perez A, Cheatham TE, Forti F, et al. Geometrical and electronic structure variability of the sugar-phosphate backbone in nucleic acids. J Phys Chem B 2008;112:8188–97.
[19] Wang J, Wolf RM, Caldwell JW, Kollman PA, Case DA. Development and testing of a general amber force field. J Comput Chem 2004;25:1157–74.
[20] Wang JM, Wang W, Kollman PA, Case DA. Automatic atom type and bond type perception in molecular mechanical calculations. J Mol Graph Model 2006;25:247–60.
[21] Berendsen HJC, Postma JPM, Vangunsteren WF, Dinola A, Haak JR. Molecular-dynamics with coupling to an external bath. J Chem Phys 1984;81:3684–90.
[22] Beeman D. Some multistep methods for use in molecular-dynamics calculations. J Comput Phys 1976;20:130–9.
[23] Ryckaert JP, Ciccotti G, Berendsen HJC. Numerical-integration of cartesian equations of motion of a system with constraints - molecular-dynamics of n-alkanes. J Comput Phys 1977;23:327–41.
[24] Lee CT, Yang WT, Parr RG. Development of the colle-salvetti correlation-energy formula into a functional of the electron-density. Phys Rev B 1988;37:785–9.
[25] Jang TS. A new functional iterative algorithm for the regularized long-wave equation using an integral equation flormalism. J Sci Comput 2018;74:1504–32.
[26] Stewart JJP. Special issue - mopac - a semiempirical molecular-orbital program. J Comput Aid Mol Des 1990;4:1–45.
[27] Ditchfield R, Hehre WJ, Pople JA. Self-consistent molecular-orbital methods .9. extended gaussian-type basis for molecular-orbital studies of organic molecules. J Chem Phys 1971;54:724–8.
[28] Mclean AD, Chandler GS. Contracted Gaussian-Basis Sets for Molecular Calculations .1. 2nd Row Atoms, Z=11-18. J Chem Phys 1980;72:5639–48.
[29] Boys SF, Bernardi F. Calculation of small molecular interactions by differences of separate total energies - some procedures with reduced errors. Mol Phys 1970;19:553–66.
[30] Simon S, Duran M, Dannenberg JJ. How does basis set superposition error change the potential surfaces for hydrogen bonded dimers? J Chem Phys 1996;105:11024–31.
[31] Ma CM, Zhao XH. Depicting the non-covalent interaction of whey proteins with galangin or genistein using the multi-spectroscopic techniques and molecular docking. Foods 2019;8:1–13.
[32] Xie JH, Ren YM, Xiao YH, Luo Y, Shen MY. Interactions between tapioca starch and Mesona chinensis polysaccharide: Effects of urea and NaCl. Food Hydrocolloid 2021;111:1–8.
[33] Yang S, Zhang B, Gong X, Wang T, Liu Y, Zhang N. *In vivo* biodistribution, biocompatibility, and efficacy of sorafenib-loaded lipid-based nanosuspensions evaluated experimentally in cancer. Int J Nanomed 2016;11:2329–43.
[34] Xiao Y, Liu Y, Yang S, Zhang B, Wang T, Jiang D, et al. Sorafenib and gadolinium co-loaded liposomes for drug delivery and MRI-guided HCC treatment. Colloids Surf. B 2016;141:83–92.
[35] Lin Ts T, Gao DY, Liu YC, Sung YC, Wan D, Liu JY, et al. Development and characterization of sorafenib-loaded PLGA nanoparticles for the systemic treatment of liver fibrosis. J control release 2016;221:62–70.
[36] Poojari R, Kini S, Srivastava R, Panda D. Intracellular interactions of electrostatically mediated layer-by-layer assembled polyelectrolytes based sorafenib nanoparticles in oral cancer cells. Colloids Surf. B 2016;143:131–8.

[37] Cao H, Wang Y, He X, Zhang Z, Yin Q, Chen Y, et al. Codelivery of sorafenib and curcumin by directed self-assembled nanoparticles enhances therapeutic effect on hepatocellular carcinoma. Mol Pharmaceut 2015;12:922–31.
[38] Zhang Z, Niu B, Chen J, He X, Bao X, Zhu J, et al. The use of lipid-coated nanodiamond to improve bioavailability and efficacy of sorafenib in resisting metastasis of gastric cancer. Biomaterials 2014;35:4565–72.
[39] Mu S, Liu Y, Wang T, Zhang J, Jiang D, Yu X, et al. Unsaturated nitrogen-rich polymer poly(l-histidine) gated reversibly switchable mesoporous silica nanoparticles using "graft to" strategy for drug controlled release. Acta biomaterialia 2017;63:150–62.
[40] Hu SQ, Lee E, Wang C, Wang JQ, Zhou ZX, Li YX, et al. Amphiphilic drugs as surfactants to fabricate excipient-free stable nanodispersions of hydrophobic drugs for cancer chemotherapy. J Control Release 2015;220:175–9.
[41] Zhao YY, Chen F, Pan YM, Li ZP, Xue XD, Okeke CI, et al. Nanodrug formed by coassembly of dual anticancer drugs to inhibit cancer cell drug resistance. Acs appl mater inter 2015;7:19295–305.
[42] Chen F, Zhao Y, Pan Y, Xue X, Zhang X, Kumar A, et al. Synergistically enhanced therapeutic effect of a carrier-free HCPT/DOX nanodrug on breast cancer cells through improved cellular drug accumulation. Mol Pharmaceut 2015;12:2237–44.
[43] Li Y, Liu GH, Ma JY, Lin JY, Lin HR, Su GH, et al. Chemotherapeutic drug-photothermal agent co-self-assembling nanoparticles for near-infrared fluorescence and photoacoustic dual-modal imaging-guided chemo-photothermal synergistic therapy. J Control Release 2017;258:95–107.
[44] Jiang K, Han LY, Guo Y, Zheng GR, Fan LL, Shen ZC, et al. A carrier-free dual-drug nanodelivery system functionalized with aptamer specific targeting HER2-overexpressing cancer cells. J Mater Chem B 2017;5:9121–9.
[45] Zhang R, Xing R, Jiao T, Ma K, Chen C, Ma G, et al. Carrier-free, chemophotodynamic dual nanodrugs via self-assembly for synergistic antitumor therapy. Acs appl mater inter 2016;8:13262–9.